

**Polar Direct-Drive Simulations for a Laser-Driven  
HYLIFE-II Fusion Reactor**

**Katherine Manfred**

**Polar Direct-Drive Simulations for a Laser-Driven  
HYLIFE-II Fusion Reactor**

Katherine M. Manfred

**Fairport High School**  
Fairport, New York

Advisor: Dr. R. S. Craxton

**Laboratory for Laser Energetics**  
University of Rochester  
Rochester, New York

November 2007

## Abstract

This report explores the possibility of using laser-driven fusion on the HYLIFE-II fusion reactor, which was originally designed for ion beam fusion. The reactor design surrounds the imploding hydrogen-containing target with a fluid waterfall, which limits any laser beams irradiating the target to  $20^\circ$  or less from a central axis. Difficulties in irradiating the equator of the target with oblique rays are overcome by concentrating beams on the equator and adjusting beam variables, such as focal spot shape and beam pointing shifts, during the laser pulse. Simulations performed using the hydrodynamics code SAGE show that it is possible, using a 2.1 MJ KrF laser, to achieve an implosion in a HYLIFE-II reactor similar to that of a design for the 1.5 MJ laser at the National Ignition Facility (NIF). This result demonstrates that laser-driven fusion may be viable on the HYLIFE-II reactor.

## 1. Introduction

Nuclear fusion has the potential to become a major source of energy in the future. Fusion involves the combination of two nuclei to release energy. In inertial confinement fusion, a driving force deposits a large amount of energy on the surface of a target, typically a thin shell surrounding the fusion fuel, causing the shell to expand rapidly. The reaction force of this rapid expansion compresses the fuel in the center of the target to very high densities and temperatures. These conditions allow the atomic nuclei to overcome electrostatic repulsion and fuse. Deuterium and tritium, two isotopes of hydrogen, are commonly used as fuel and react according to the equation  $D + T \rightarrow {}^4\text{He} (3.5 \text{ MeV}) + n (14.1 \text{ MeV})$ . The kinetic energy of the neutron is the main output energy. If there is a sufficient amount of fuel at a high density, the helium nucleus deposits its energy in the fuel, providing energy for more fusion reactions. This state of sustained

reactions is known as ignition. For fusion energy to be usable as a source of energy, the fuel must ignite in order to generate a larger amount of energy than is required to initiate the reaction.

Three approaches to inertial confinement fusion are shown in figure 1.1. They involve two broad categories of driving forces: heavy ion beams<sup>1</sup> and lasers<sup>2</sup>. In ion-beam fusion [see figure 1.1(a)], ions are accelerated and compressed in time to form short pulses that pass through the wall of the hohlraum, a gold cylinder surrounding a target. The ions deposit their energy in a thick metal plate, which emits x rays that irradiate the target within the hohlraum. In direct-drive laser fusion [see figure 1.1(b)] the shell of the target absorbs energy from an array of laser beams focused on the target from many sides. Indirect-drive laser fusion [see figure 1.1(c)] involves using laser beams pointed at the inner walls of a hohlraum. The hohlraum absorbs the energy and emits x rays, which irradiate the target.

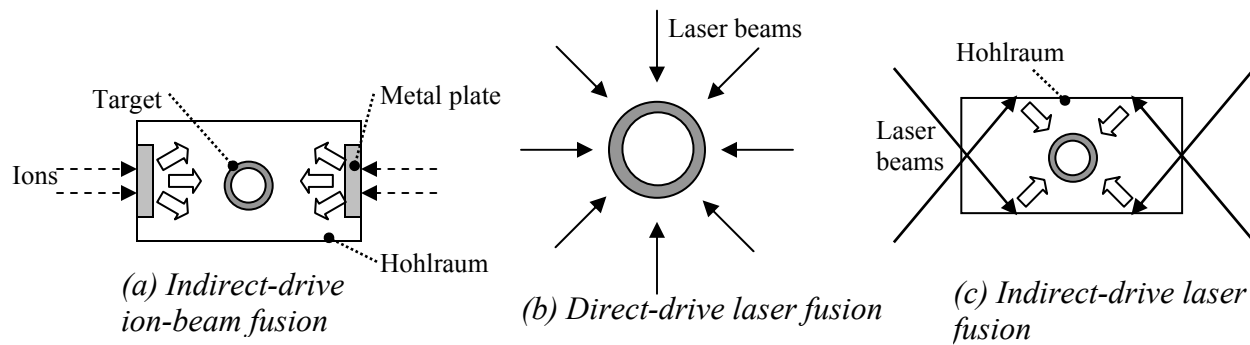


*Figure 1.1: Three approaches to inertial confinement fusion: (a) Ion beam energy is absorbed by a thick metal plate, causing it to emit x rays (block arrows) that are confined within the hohlraum and irradiate the target. (b) Laser beams are directly incident on the surface of the target. (c) Laser energy is incident upon the inner wall of the hohlraum to produce x rays that irradiate the target.*

The High-Yield Lithium-Injection Fusion-Energy (HYLIFE)-II<sup>3,4</sup> fusion reactor design [Figure 1.2(a)] presents an innovative method for harnessing the energy of nuclear fusion reactions. In conventional fusion reactor designs, the wall of the chamber must withstand repeated bombardments by neutrons, x rays, and debris from the reaction. These walls would

have to be replaced quite often to maintain the integrity of the chamber. The HYLIFE-II chamber design, however, features a liquid lithium salt ( $\text{Li}_2\text{BeF}_4$ ) cascade, which protects the structure wall from x ray damage and debris. This liquid flows down from oscillating jets to form pockets around each imploding target. High-velocity neutrons emitted by the fusion reactions are absorbed by the fluid as it flows around the target. The heat gained from this absorption is then used to turn turbines and produce usable power. The neutrons react with lithium to produce tritium atoms according to the equation  ${}^7\text{Li} + n \rightarrow {}^4\text{He} + \text{T} + n$ . The tritium bred in the liquid lithium is an important source for the fuel since naturally occurring tritium is rare. The HYLIFE-II reactor was initially designed for heavy ion beam fusion. The ion beams would be pointed

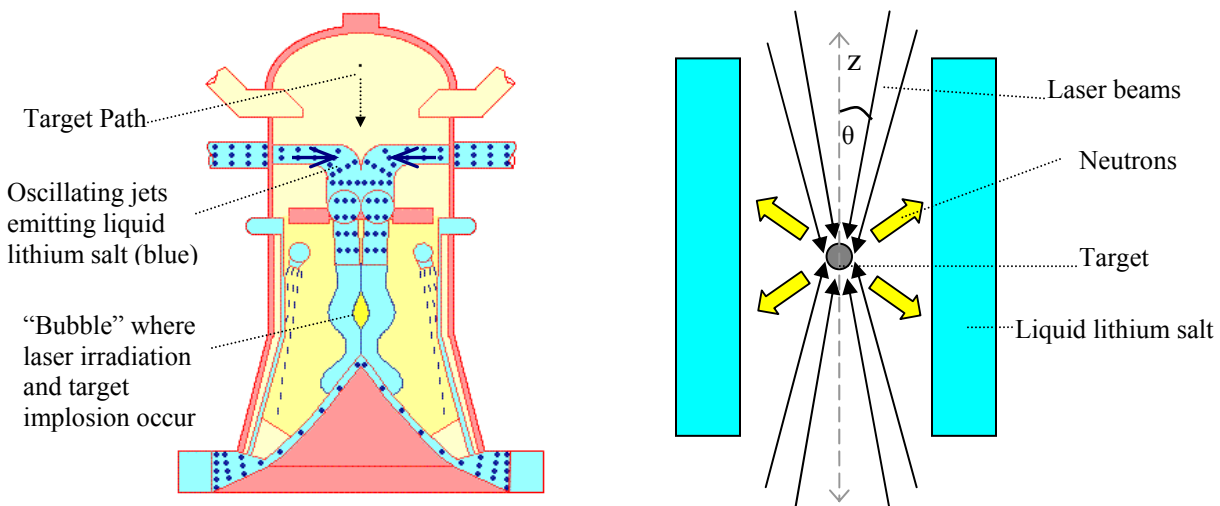


Figure 1.2: (a) Front view of HYLIFE-II reactor design. The target is injected from the top of the chamber and imploded while surrounded by the liquid. (from Ref. 5)

(b) Overhead view of the target while enclosed in lithium salt [perpendicular to Figure 1.2 (a)] Laser beams must enter with  $\theta \leq 20^\circ$ .

at the hohlraum that surrounds the target through a single, narrow aperture in the fluid. Since a narrow break in the fluid is needed for the ion beams to irradiate the hohlraum, only a small portion of the chamber would be unprotected by the liquid cascade.

Laser systems have been used extensively in fusion experiments, a significant advantage

over ion beam drivers. The use of lasers with the HYLIFE-II reactor has previously been considered impossible because the laser beam arrangement is restricted by the liquid lithium flow in the chamber. In order for the liquid to absorb at least 90% of the emitted neutrons, the laser beams must enter the pocket perpendicular to the direction of flow at angles of  $20^\circ$  or less from the central axis [figure 1.2 (b)]. Indirect-drive cannot be adapted to these requirements since current designs require laser beam angles of  $23^\circ$  to  $50^\circ$  to irradiate the interior walls of the hohlraum. This work explores the possibility of using direct-drive laser fusion on the HYLIFE-II reactor. The results show that this method has the potential to be very successful.

## 2. Polar Direct-Drive

The method of using direct drive from two opposing sides of the target, termed polar direct-drive (PDD), has been previously developed<sup>6-9</sup> for the National Ignition Facility (NIF). The NIF, set to be fully operational in 2010, is a 1.8 MJ neodymium-doped glass laser with four

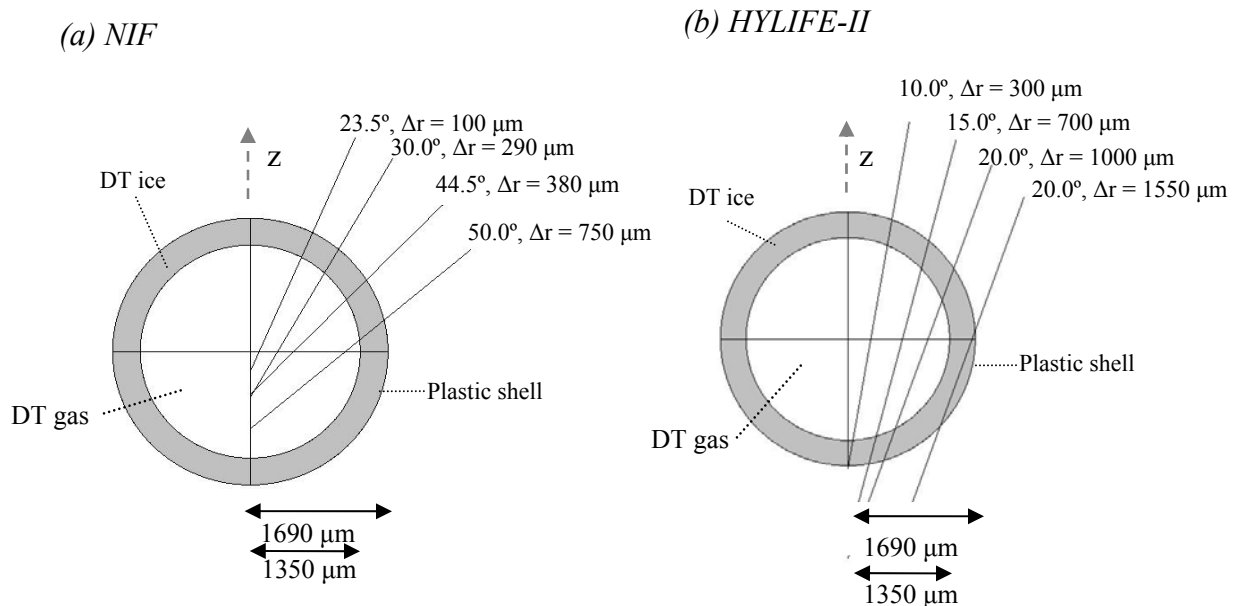


Figure 2.1 (a) Beam pointing arrangement for a direct-drive NIF design. (b) Initial beam pointing proposed for the HYLIFE-II design. Both designs use the same cryogenic DT target.

rings of laser beams that enter from the top of the target chamber and four rings symmetrically aligned on the bottom. The rings are arranged at angles of  $23.5^\circ$ ,  $30.0^\circ$ ,  $44.5^\circ$ , and  $50.0^\circ$  from the vertical [see Figure 2.1(a)] with relative energies of 4:4:8:8, respectively. This arrangement was constructed specifically for indirect-drive experiments, but a PDD design was developed to use the NIF for direct-drive implosions. In this design, beams are shifted away from the center of the target by amounts  $\Delta r$ , measured perpendicular to the laser path. This shift allows laser energy to be deposited evenly across the surface of the target, including the equatorial plane.

In contrast, it is difficult to balance the energy absorbed across the surface using the shallow laser beam angles required for the HYLIFE-II reactor. To explore this, a HYLIFE-II design [see figure 2.1(b)] was developed using the same target used on the NIF; thus the design can be compared to the PDD design for the NIF in order to analyze uniformity and implosion velocity. The target<sup>10</sup> used in these designs is comprised of a plastic (CH) shell surrounding a thick ( $340\ \mu\text{m}$ ) layer of deuterium-tritium (DT) ice and DT gas with a total diameter of  $3380\ \mu\text{m}$ . Targets are produced and maintained at cryogenic temperatures until injected into the reactor.

### **3. Design for HYLIFE-II Reactor**

The proposed design assumes a krypton fluoride (KrF) laser<sup>11</sup> power source. The KrF laser has the ability to allow multiple changes to beam shifting and focal spot shape during the pulse, a flexibility not currently available with glass lasers such as the NIF. Separate laser pulses are passed sequentially through apodizers, which shift the pointing and establish the spatial profile of each pulse. The shorter wavelength of the KrF laser also allows it to penetrate further into the imploding target than traditional glass lasers, thus increasing absorption.

The proposed laser arrangement features two symmetrical clusters of four laser beam

rings with angles of  $10^\circ$ ,  $15^\circ$ ,  $20^\circ$ , and  $20^\circ$ , respectively [see figure 2.1(b)] The intensity ratio for the four rings is 1.5:6:8:20. This design uses a 2.1 MJ KrF laser to achieve very similar results to the PDD design for the NIF, which uses 1.5 MJ of energy. The additional KrF energy is necessary to overcome the decreased absorption due to the oblique angle of some of the laser beams. These beams deposit energy in lower density plasma surrounding the target and the target is not able to absorb the laser energy effectively. Figure 3.1 shows the incident and absorbed power over time. The HYLIFE-II design only absorbs about 44% of the entire energy incident upon the target compared to the  $\sim 60\%$  absorption of the NIF design. Thus, more energy is required to ensure that the implosion takes place at the same rate. Changes to the beam shifting and focal spot shape are made at the times indicated in the figure to provide the maximum absorption and uniformity over short time intervals.

In PDD designs, laser beam pointing is shifted away from the center of the target in order to irradiate the shell uniformly, as shown in figure 2.1. The shifts are made by adjusting the locations of the apodizers at the front end of the laser system. Since the HYLIFE-II design

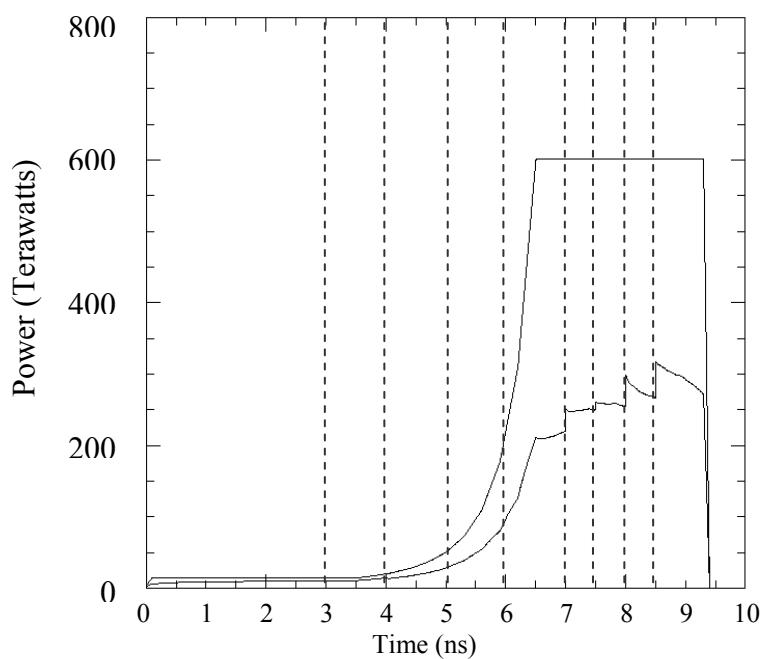


*Figure 3.1: Laser power incident on the target (top curve) and absorbed (bottom curve) over the course of the laser pulse. The dashed vertical lines represent times during the laser pulse when adjustments are made to beam pointing and focal spot shape.*

requires much shallower angles than the NIF design, the challenges of irradiating the target surface evenly are increased. It is necessary to alter the shifts many times during the laser pulse. Figure 3.2 illustrates the shifts made to the outer ring of laser beams. This ring moves in as the target implodes to ensure that the equator absorbs an effective amount of energy. If the original beam pointing were maintained, much of the outer laser beam energy would not irradiate the target shell but merely pass by the target at a later time, as shown by the dashed green line in figure 3.2 (b).

The intensity is assumed to be a generalized Gaussian proportional to  $\exp(-(r/r_0)^n)$  at radius  $r$  with  $n = 2.5$  (see figure 3.3). The  $r_0$  value affects the radius of the beam and is only altered in the outermost ring of beams from 1000  $\mu\text{m}$  to 900  $\mu\text{m}$ . Narrower beams, with lower  $r_0$  values, can be used when small portions of the target need to be driven in more. Wider beams, with larger  $r_0$  values, ensure an effective overlap of beams in the azimuthal ( $\phi$ ) direction. The ellipticity of the focal spot can also be adjusted, and is the primary means of reducing the size of the beams. The focal spot is compressed along the  $z$  axis to form varying degrees of ellipticity without affecting the radius in the  $\phi$  direction. As with the other variables, this is adjusted by the

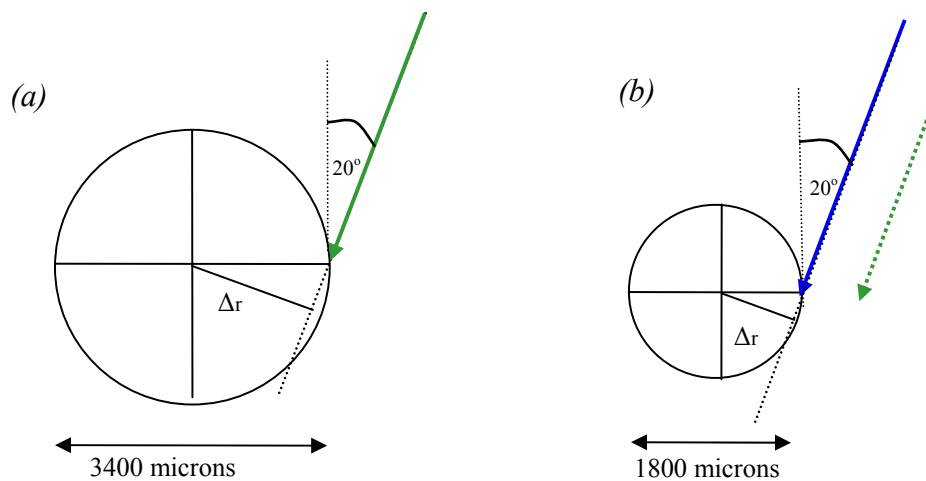
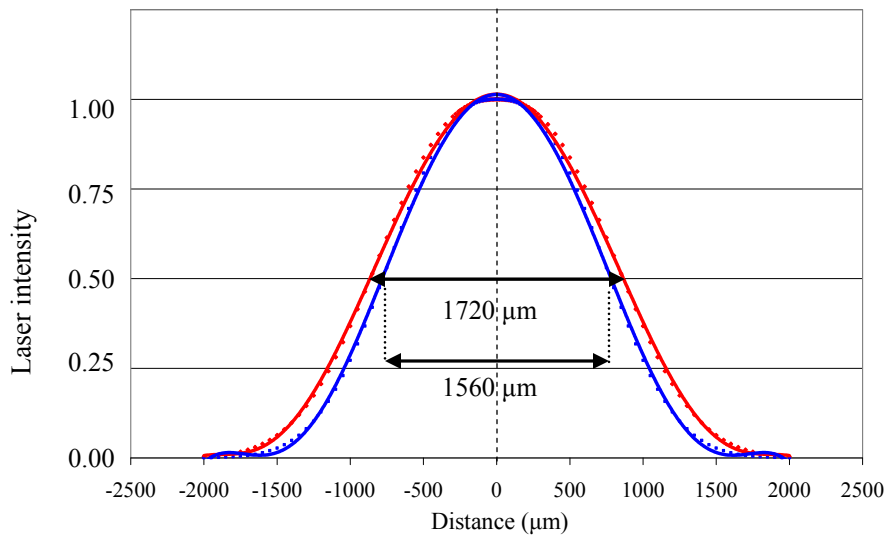


Figure 3.2 (a) Initial target and initial pointing of the outer laser beams. (b) Imploded target about 9 ns into the simulation with the new beam pointing (blue) and the original beam pointing (green).



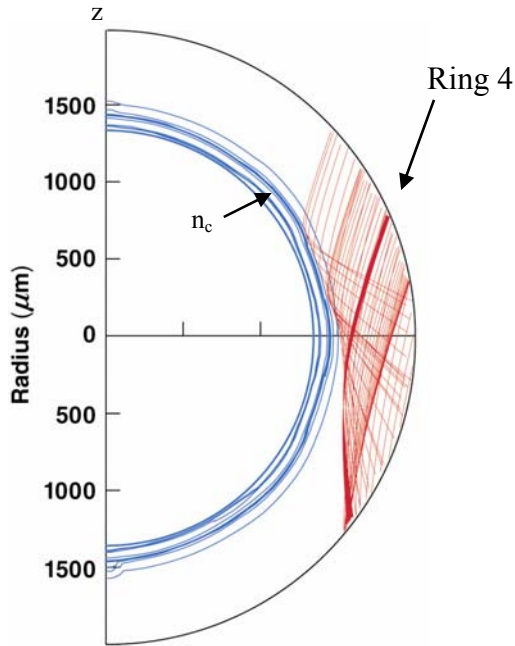
*Figure 3.3: Intensity of laser beam as a function of the distance from the center of the focal spot. The wider beam (red) has an  $r_o$  value of  $1000\ \mu\text{m}$  and the narrower beam (blue) has an  $r_o$  value of  $900\ \mu\text{m}$ .*

apodizers near the laser source. The laser beam specifications are found in the Appendix.

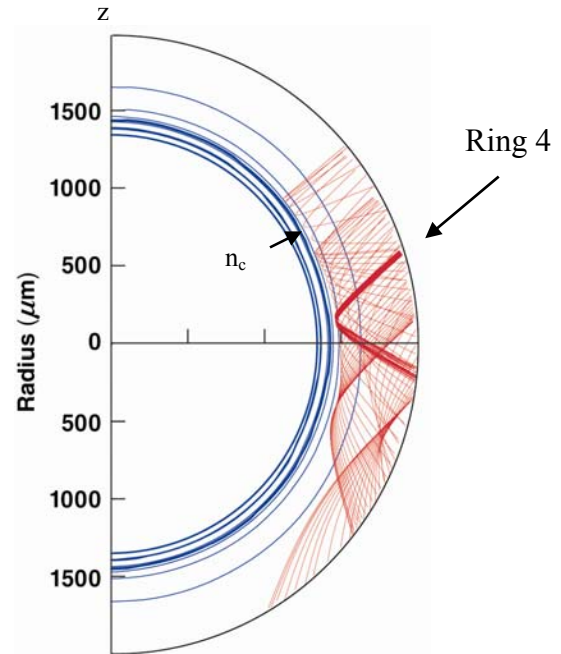
Figure 3.4 (a) shows density contours of the HYLIFE-II design at 5.8 ns. Laser rays from the outermost ring are also shown. The less oblique laser rays penetrate close to the critical density, the maximum density at which the laser beam can deposit energy. The more oblique rays deposit energy in the hot plasma surrounding the target. This energy cannot effectively drive the implosion of the target shell. There is an obvious weakness at the equator of the HYLIFE-II design due to this ineffective absorption of oblique rays. At about  $70^\circ$  from the pole, there is a region of the shell that experiences a higher velocity. This area absorbs energy effectively from the outer parts of laser beams pointed at the equator because these rays hit the surface more directly. Over time, this irregularity exacerbates the weakness at the equator. As the regions around the equator implode faster, mass is pushed toward the equator. The amount of energy deposited on the equator therefore needs to be increased over the course of the implosion to compensate for this increased mass.

Figure 3.4 (b) shows density contours at the same time for the NIF design. The outer ring hits the target at a much higher angle to the vertical axis ( $50^\circ$ ) and the equator implodes at a

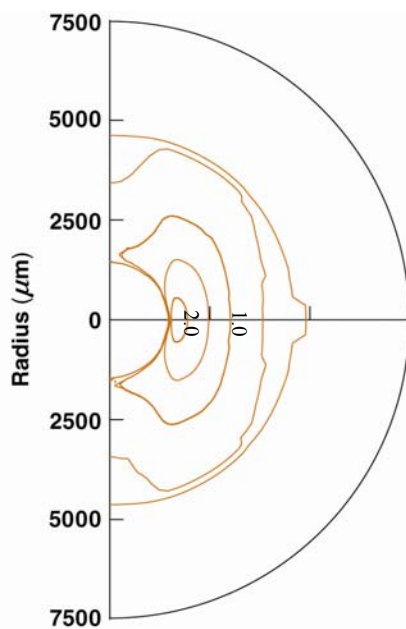
(a) HYLIFE-II: Density Contours (5.8 ns)



(b) NIF: Density Contours (5.8 ns)



(c) HYLIFE-II: Temperature Contours



(d) NIF: Temperature Contours

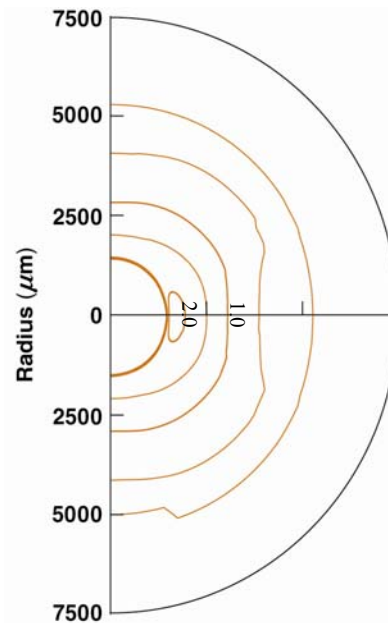
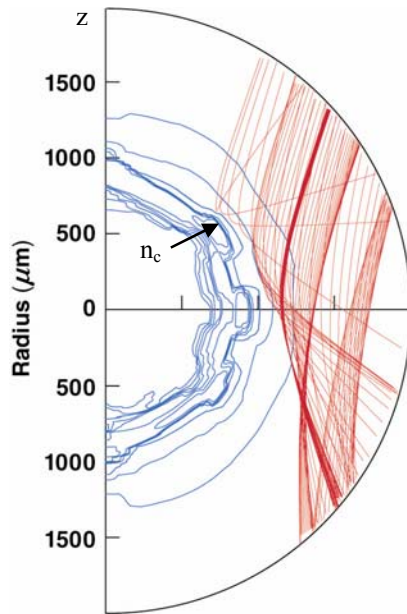


Figure 3.4: (a) Density contours of the HYLIFE-II target at 5.8 ns with rays from an outer laser beam. The critical density ( $n_c$ ), or the maximum electron density to which the laser can penetrate, is also shown. (b) Density contours of the NIF design at the same time. In these plots azimuthal symmetry about the  $z$  axis is assumed. (c) Temperature contour plot (keV) of the HYLIFE-II design at 5.8 ns. The maximum temperature is 2.5 keV. (d) Temperature contours of the NIF design with a maximum temperature of 2.1 keV.

(a) HYLIFE-II: Density Contours (9 ns)



(b) NIF: Density Contours (9 ns)

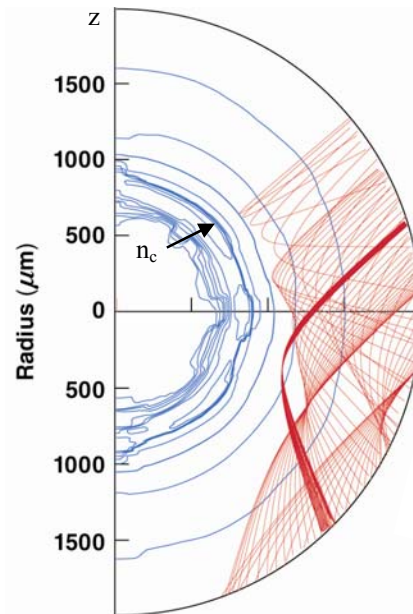


Figure 3.5: (a) Density contours of the HYLIFE-II design at 9 ns showing rays of the outer laser beam ring. Azimuthal symmetry is assumed about the  $z$  axis. (b) Same for the NIF design at 9 ns.

higher velocity at this point in the simulation. The overall uniformity is better than that of the HYLIFE-II design at this time.

The temperature contours [see figure 3.4 (c) and (d)] of the two designs are very similar; however, the HYLIFE-II design experiences a higher maximum temperature near the equator: 2.5 keV versus 2.1 keV for the NIF design. Both maxima occur very near the equator of the target; however, the HYLIFE-II design experiences a greater temperature difference between the poles and equator. Since hot plasma absorbs laser energy less efficiently, this high temperature further intensifies the nonuniformity at the equator on the HYLIFE-II design.

Density contours of the designs at 9 ns are shown in figure 3.5. The HYLIFE-II design maintains an approximately spherical shape as it implodes. There are three weak points in the

target where the mass has imploded slower than in adjacent regions, which mirror similar regions of nonuniformity in the NIF design [see figure 3.5 (b)]. In both designs, the target has imploded to about half its original size by this time.

Figure 3.6 shows the center of mass radius of the imploding shell as a function of angle  $\theta$  measured from the vertical pole ( $z$  axis) for the HYLIFE-II design at three times and the NIF design at 9 ns. The root-mean-square (rms) deviation of the radius is calculated by averaging the radius over the surface of the target. The deviation of the radius increases from  $7.1 \mu\text{m}$  at 5.8 ns to  $32 \mu\text{m}$  at 9 ns. Though the deviation at 9 ns is considerably higher than the NIF deviation of  $12.0 \mu\text{m}$ , it is small compared with the  $900 \mu\text{m}$  decrease in target radius. Both designs share similar weak points, specifically around the equator and at  $\theta \sim 60^\circ$  from the poles. These irregularities appear even at very early times and only intensify during the implosion.

Figure 3.7 shows the inward velocity of the target as a function of angle  $\theta$  for the HYLIFE-II and NIF designs, at the same times as figure 3.6. Consistent velocity across the

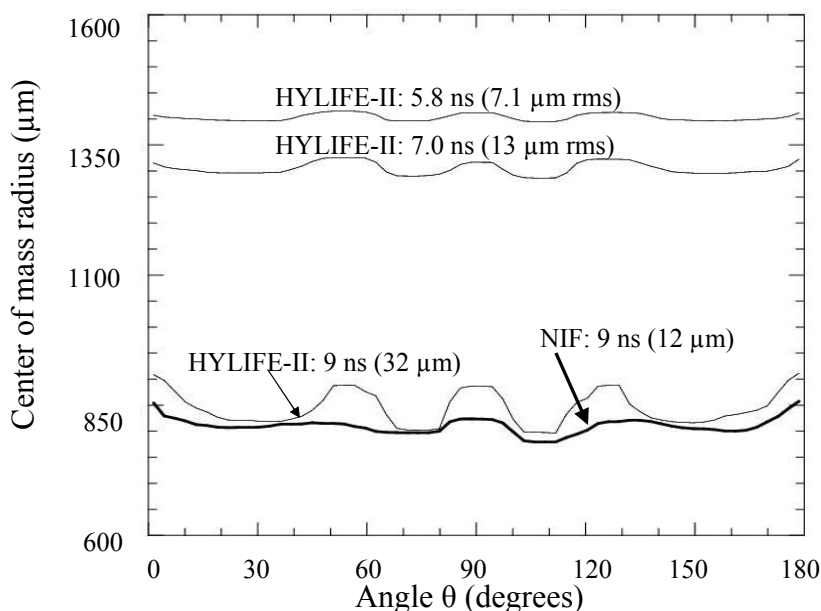


*Figure 3.6: The center of mass radius versus angle from the vertical pole. The average center of mass radius at 9 ns for the HYLIFE-II design is very similar to the NIF design at 9 ns (bold line).*

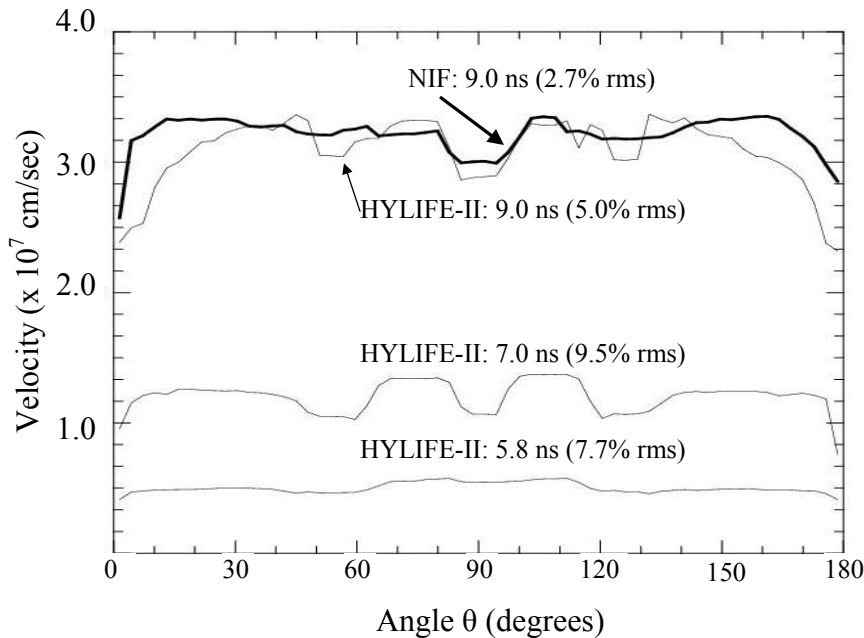


Figure 3.7: The average inward velocity of the imploding target versus angle  $\theta$  from the pole at the same times as figure 3.6. Velocity uniformity remains fairly good throughout the implosion and is comparable to that of the NIF design at 9 ns.

surface of the target demonstrates a balanced distribution of driving energy across the target shell. The average velocities of the two target designs near the end of the laser pulse are quite similar:  $3.1 \times 10^7$  cm/sec for the HYLIFE-II design and  $3.2 \times 10^7$  cm/sec for the NIF design at 9 ns. Though the 5.0% velocity rms for the HYLIFE-II design is higher than the 2.7% rms of the NIF design, some of this nonuniformity is due to slower implosion at the poles. With a few minor refinements to the design, this deficiency can probably be eliminated.

#### 4. Optimization

Over a thousand simulations were conducted using the hydrodynamics code SAGE<sup>12</sup> to develop this design for the HYLIFE-II reactor. The design was developed by optimizing each time interval successively by analyzing graphs such as Figures 3.6 and 3.7. Beam specifications for each interval would often produce good uniformity early in the interval that would deteriorate as time progressed, leading to the need to create the next interval. The optimized design requires nine time intervals. Fewer than nine intervals were found to lead to a sharp increase in shell

irregularities. Figure 4.1 shows a comparison between the uniformity at 5.8 ns of the optimized design and a similar design with one less time interval. The unoptimized design, produced by delaying a large move of the third ring of laser beams for a nanosecond, yielded a very nonuniform implosion.

Figure 4.2 shows the degree to which beam shifting and focal spot shape are changed on two different beams. The pointing shift of the outermost ring is shown in figure 4.2 (a). As the target implodes and the core compresses, the outer ring of laser beams shifts often to maintain its focus on the equator. This ring moves from an initial position of 1550  $\mu\text{m}$  from the center of the target to 900  $\mu\text{m}$  at 9 ns. Larger changes are made at later times in the pulse when the target is imploding at a higher velocity and becomes more sensitive to pointing changes.

Figure 4.2 (b) shows the increasing ellipticity of the laser beams in the third ring. Circular focal spot shapes are used at early times so that the overlapping of multiple beams can

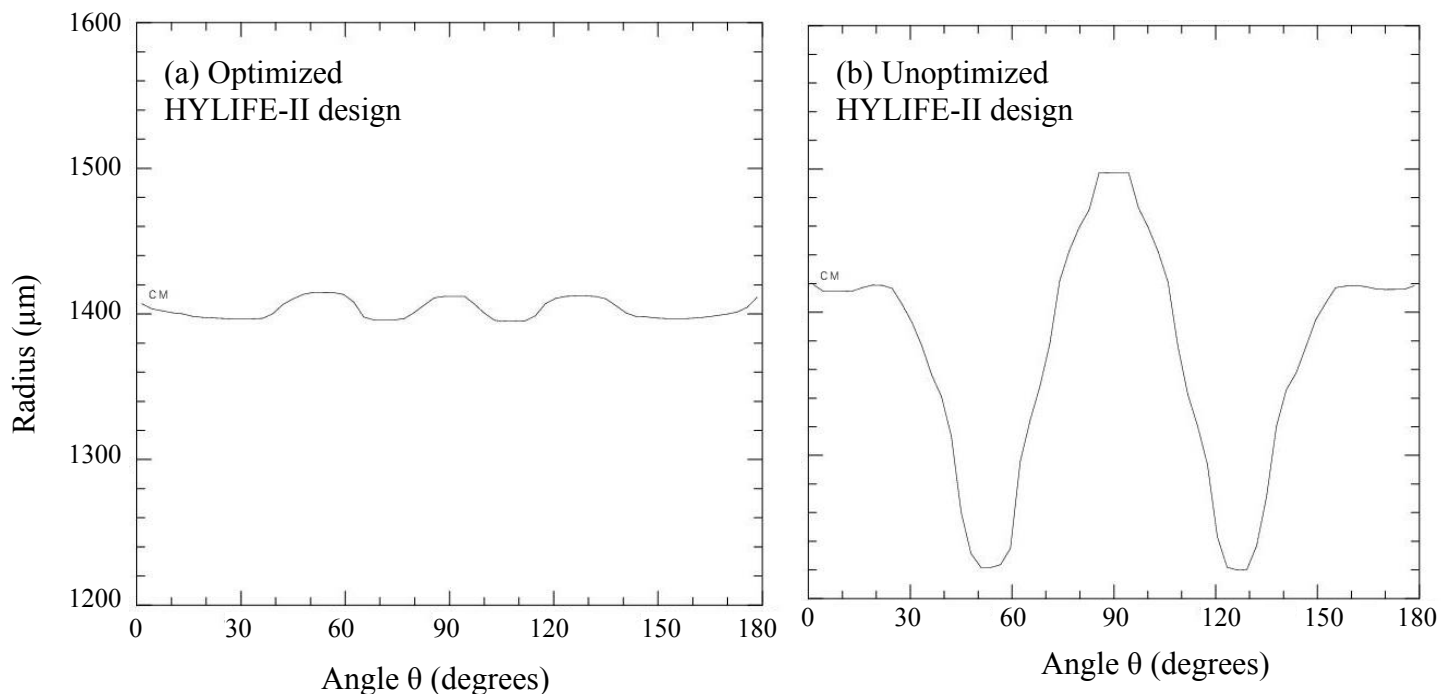


Figure 4.1: (a) Center of mass radius as a function of  $\theta$  at 5.8 ns for the HYLIFE-II design. (b) Center of mass radius for the same time using one less time interval.

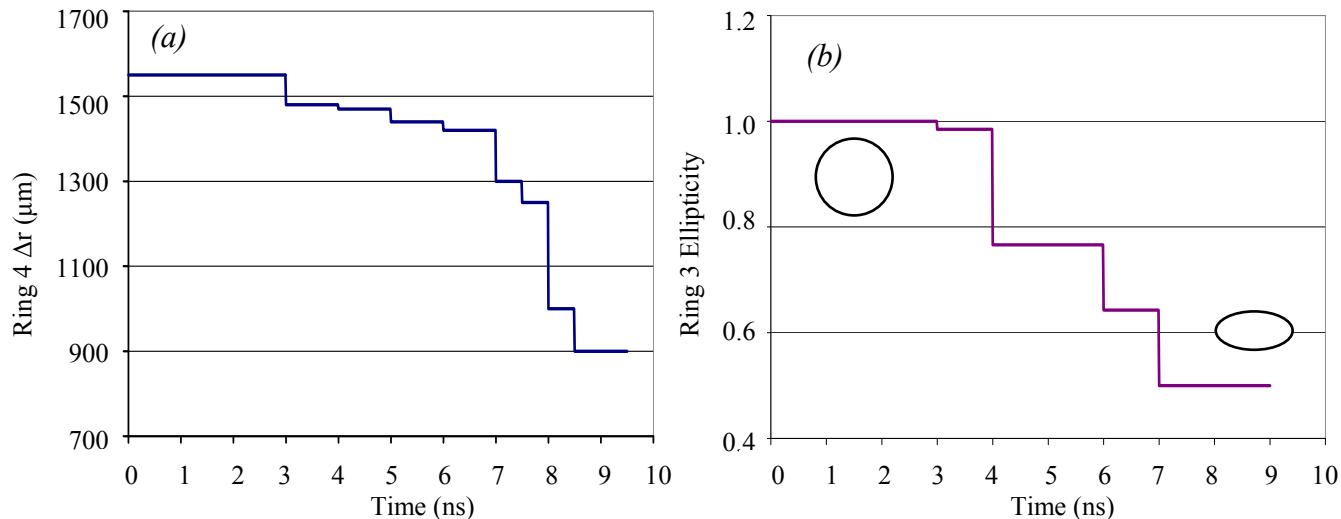


Figure 4.2: (a) Beam shifts of the outermost laser beam ring over the course of the laser pulse. (b) Ellipticity (b:a ratio) of the focal spots of ring 3 beams as a function of time. The insets show visual representations of the initial shape (circular) and final shape (elliptical).

smooth out the energy deposition across the surface of the target. At later times, however, beam shapes flattened in the z direction are required. Beams in the second and third ring require the most adjustment to the focal spot shape as the target implodes. The outermost laser beam ring maintains a very elliptical spot in order to concentrate energy on a narrow band around the equator, while inner beams, in general, have a more circular spot shape.

## 5. Conclusions

A laser-driven target design suitable for the HYLIFE-II reactor was developed using hydrodynamic simulations. The level of flexibility offered by a KrF laser allows adjustments to beam shifting and focal spot shape over several intervals throughout the course of the laser pulse. By adjusting these parameters, a design was developed in which the target implodes to half its original radius with a velocity root-mean-square nonuniformity of 5.0%.

Further explorations are required to develop an ideal configuration. Many possible variables were not explored extensively, such as different laser beam angles within the 20° limitation, the number of laser beam rings, and the n parameter affecting the focal spot shape. Simulations can be conducted with different beam shapes, such as crescent-shaped focal spots. By adjusting the width and curvature of these shapes, the laser beam can wrap around the equator for more effective irradiation and absorption. A ring-shaped beam with the ring diameter approximately equal to the target diameter would also be a possible solution. This shape would provide very uniform irradiation in the  $\phi$  direction around the equator. This beam could be pointed directly along the axis of the target, thus falling well within the constraints of the reactor geometry.

Although nonuniformities in the imploding shell were not eliminated, this work shows the viability of using lasers to drive fusion reactions in the HYLIFE-II reactor. Previously, it was not considered plausible to consider a laser-driven design because the reactor requires laser beam angles of 20° and less. The initial design shows great promise for laser-driven fusion on HYLIFE-II, and it will serve as the foundation for future such designs for this reactor.

## **6. Appendix**

Specifications of the three key parameters of the HYLIFE-II design are presented in Table 6.1 with the time at which each group of variables is initiated. Each ring of beams maintains a specific angle to the central axis (z) of the target throughout the irradiation. Beam shifts, denoted by  $\Delta r$ , are measured from the center of the target perpendicular to the trajectory of the rays. The focal spot intensity is assumed to be proportional to  $\exp(-(r/r_0)^n)$  where  $n = 2.5$ . The  $r_0$  value affects the width of the focal spot, and is maintained at a moderately large value to

ensure adequate overlapping of focal spots in the azimuthal direction around the target shell.

The ellipticity ( $\epsilon$ ) is the b:a ratio of the focal spot, with b indicating the height of the focal spot produced by compressing the spot vertically.

*Table 6.1: Specification of the HYLIFE-II design presented in this report. Each change in parameter settings occurs at the time listed and is maintained until the next indicated change. ( $r_o$  = beam radius,  $\epsilon$  = ellipticity,  $\Delta r$  = beam shift.) All distances are in  $\mu\text{m}$ .*

Time (ns)	Beam 1: $10^\circ$ ( $r_o = 1000 \mu\text{m}$ )		Beam 2: $15^\circ$ ( $r_o = 1000 \mu\text{m}$ )		Beam 3: $20^\circ$ ( $r_o = 1000 \mu\text{m}$ )		Beam 4: $20^\circ$ ( $\epsilon = 0.42$ )	
	$\Delta r$	$\epsilon$	$\Delta r$	$\epsilon$	$\Delta r$	$\epsilon$	$\Delta r$	$r_o$
0.0	-300	1.00	-700	1.00	-1000	1.00	-1550	1000
3.0	-300	1.00	-600	1.00	-800	0.98	-1480	1000
4.0*	-300	1.00	-750	0.98	-1460	0.77	-1470	1000
5.0	-300	1.00	-750	0.87	-1450	0.77	-1440	1000
6.0	-200	0.99	-750	0.97	-1410	0.64	-1420	1000
7.0	-200	0.94	-720	0.77	-1310	0.50	-1300	1000
7.5	-200	0.94	-720	0.77	-1270	0.50	-1250	1000
8.0	-650	0.87	-1060	0.77	-1020	0.50	-1000	1000
8.5	-50	1.00	-650	0.87	-900	0.50	-900	900

\* This time interval was eliminated for the unoptimized HYLIFE-II design used for figure 4.1 (b).

There are noticeable discontinuities in some of the parameters, especially the shifting of the second ring of laser beams in the interval starting at 8 ns. While the parameters in Table 6.1 provided reasonable uniformity, a more continuous alternative could probably be found.

## 7. Acknowledgements

I would like to thank my advisor Dr. R. Stephen Craxton for generously sharing his time, expertise, and enthusiasm, as well as Alexandra Cok for her valuable guidance and encouragement. I would also like to thank Dr. Craxton and the entire Laboratory for Laser Energetics for providing this wonderful research opportunity.

## 8. References

1. D. Callahan, *et al.*, “Advances in Target Design for Heavy Ion Fusion.” *Plasma Phys. Control. Fusion* **47**, B379 (2005).
2. J. Nuckolls, *et al.*, “Laser Compression of Matter to Super-High Densities: Thermonuclear (CTR) Applications,” *Nature* **239**, 139 (1972).
3. R.W. Moir, “HYLIFE-II Inertial Fusion Energy Power Plant Design,” *Fusion Technology* **25**, 1475 (1992).
4. R.W. Moir, *et al.*, “HYLIFE-II: A Molten-Salt Inertial Fusion Energy Power Plant Design – Final Report,” *Fusion Technology* **25**, 5 (2004).
5. F. Peterson, “Target Chambers for Inertial Confinement Fusion”, (University of California Berkeley Department of Nuclear Engineering, Berkeley, CA, 1998), <http://www.nuc.berkeley.edu/thyd/icf/>
6. S. Skupsky, *et al.*, “Polar Direct Drive on the National Ignition Facility,” *Phys. Plasmas* **11**, 2763 (2004).
7. R.S. Craxton, *et al.*, “Polar Direct Drive: Proof-of-Principle Experiments on OMEGA and Prospects for Ignition on the National Ignition Facility,” *Phys. Plasmas* **12**, 056304 (2005).
8. R.S. Craxton and D.J. Jacobs-Perkins, “The Saturn Target for Polar Direct Drive on the National Ignition Facility,” *Phys. Review Letters* **94**, 095002 (2005).
9. J.A. Marozas, *et al.*, “Polar-Direct-Drive Simulations and Experiments,” *Phys. Plasmas* **13**, 0563311 (2006).
10. P.W. McKenty *et al.*, “Analysis of a Direct-Drive Ignition Capsule for the National Ignition Facility,” *Phys. Plasmas* **8**, 2315 (2001).

11. J.D. Sethian, *et al.*, “Electron Beam Pumped KrF Lasers for Fusion Energy,” *Phys. Plasmas* **10**, 2142 (2003).
12. R.S. Craxton and R.L. McCrory, “Hydrodynamics of Thermal Self-focusing in Laser Plasmas,” *Journal Appl. Phys.* **56**, 108 (1984).